Reconstructing Seasonal Variation of Landsat Vegetation Index Related to Leaf Area Index by Fusing with MODIS Data

Hankui Zhang, Jing M. Chen, Bo Huang, *Associate Member, IEEE*, Huihui Song, and Yiran Li

***Abstract*—In the development of an empirical relationship between the leaf area index (LAI) and the vegetation index (VI), the infrequency of the medium resolution VI often makes it difficult, sometimes impossible, to find VI observations acquired close to the LAI measurement date. To overcome this dilemma, this paper presents a method, named reduced simple ratio (RSR), to reconstruct seasonal time series of a VI at the Landsat resolution. Each RSR time series is represented by a double logistic (D-L) curve with seven unknown parameters. The methodology solves these parameters using a multi-objective optimization method by blending frequent MODIS observations with Landsat observations acquired at a few dates (usually fewer than seven) in a year. We tested the reconstructing approach in a boreal forest in Canada and a cropland area in Australia. The reconstructed Landsat RSR compared well with the observed RSR even when only two Landsat images were used for reconstruction, and better accuracy was achieved when more Landsat images were used. Ground LAI measurements were taken at a date not coincident with any of the Landsat dates in the Canada study area. Results of LAI retrieval showed that the measured LAI had a higher correlation with the reconstructed RSR at the measurement date than with the observed Landsat RSR at the three acquisition dates.**

***Index Terms*—Double logistic, fusion, leaf area index, multi-objective optimization.**

I. Introduction

LEAF AREA INDEX (LAI) is defined as half the total (all-sided) green leaf area per unit ground area [1]. It is an important biophysical parameter for process-based models for various purposes including plant growth estimation, numerical weather forecast, and hydrological and ecological studies. Various studies have found fairly strong relationships between LAI and vegetation indices (VIs), such as normalized difference vegetation index [2], simple ratio (SR) [3], infrared simple ratio [4], and reduced simple ratio (RSR) [5]. The superior performance of RSR for LAI estimation in coniferous stands over other VIs is supported by results in [6]–[12] and in deciduous stands in [5], [13]. And RSR has been used for LAI mapping at the regional scale [14], [15]. To develop the relationship between LAI and VI, the VI must be frequent enough to adapt to the arbitrary of the LAI measurement dates. Coarse spatial resolution (250–7000 m) data provide favorable data sources for the retrieval of high temporal resolution VI. However, the spatial heterogeneity within a pixel is a main cause for the distortion of the LAI retrieval from coarse resolution data [13], [16], [17]. Optical sensors at medium resolutions (10–100 m) can provide spatial information at the required resolutions [13], but their temporal resolution is lacking. Thus, in previous studies [7], [8], [13], the relationship between LAI and RSR was usually established using Landsat images acquired at different dates from the LAI measurement date.

This intrinsic tradeoff between the spatial and temporal resolutions of satellite data has motivated the exploration of various techniques to fuse satellite images from multiple sensors to generate high spatial and temporal resolution data. Different from data assimilation, these techniques try to integrate data from other satellites bearing complementary characteristics [18]–[24] rather than to integrate physical models [25]. The spatial and temporal adaptive reflectance fusion model, which blends TM/ETM+ and MODIS data to generate synthetic Landsat-like imagery on a daily basis [19], represents a significant step in this direction. Huang and Song [20] proposed a SParse-representation-based SpatioTemporal reflectance Fusion Model to form a unified framework for fusing remote sensing images with both phenology change and cover type change. Neither of them utilized temporal information of vegetation phenological profiles from the frequent low-resolution data. The seasonal variation in the VI has been described by using double logistic (D-L) functions [21], [22], which have created superior performance to the other describing functions [23]. Recently, Gray and Song [24] reconstructed time series of Landsat data through two Landsat observations at the growing season by using the D-L function. However, this method has two limitations: 1) the number of Landsat acquisitions for the reconstruction is limited to two which must be observed when VI is at its minima and maxima values of the growing period; and 2) it assumed that VIs in all Landsat pixels are only different at minima and maxima VI values in the phenology

Manuscript received February 08, 2013; revised April 20, 2013; accepted September 26, 2013. Date of publication October 21, 2013; date of current version March 14, 2014. This research was supported by a grant (2010CB950704) from the Global Change Key Program of Science and Technology.

H. Zhang, B. Huang, and H. Song are with Department of Geography and Resource Management, The Chinese University of Hong Kong (CUHK), Shatin, NT, Hong Kong.

J. M. Chen is with the Department of Geography and Program in Planning, University of Toronto, Toronto, ON, Canada M5S 3G3 (e-mail: chenj@geog.utoronto.ca).

Y. Li is with the Department of Systems Engineering and Engineering Management, The Chinese University of Hong Kong (CUHK), Shatin, NT, Hong Kong.

Color versions of one or more of the figures in this paper are available online at http://ieeexplore.ieee.org.

Digital Object Identifier 10.1109/JSTARS.2013.2284528

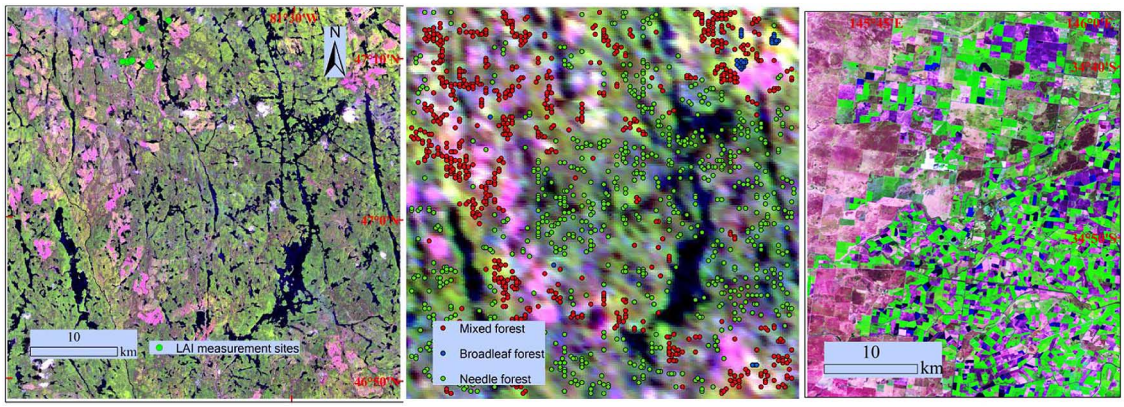

Fig. 1. The left and right images show the TM middle-infrared, near-infrared, and red bands in R/G/B composite acquired on June 16, 2009 for the Canada study area and on October 7, 2001 for the Australia study area, respectively. The middle image shows the corresponding bands of the 16-day MODIS NBAR composite (August 21–September 5) resampled to 250 m for the Canada study area. Green, blue, and red dots correspond to the valid MODIS sampling after eliminating the extraordinary samples (Section II-C).

trajectory and thus ignored the other difference in phenology metrics like on-set of green dates, rate of green-up, rate of withering, etc.

To address these problems, this paper presents a novel spatial temporal fusion method to reconstruct the seasonal time series VI at the Landsat resolution. To account for the phenology variance within a vegetation type [22], the proposed method models its variation behavior as that the fitted D-L parameters for all individuals of time series data follow a statistical (e.g., Gaussian) distribution [26]. To fuse seasonal time series of MODIS data and Landsat data acquired at arbitrary date(s) within a year, the methodology is based on a multi-objective optimization technique.

II. Test Site and Data Preprocessing

A. Test Site and Samples

The first study area is located at a boreal forest near Sudbury, Ontario, Canada, with 90×90 MODIS 500 m pixels (Fig. 1), which is covered by diverse boreal vegetation types, including deciduous and evergreen forests based on the 2005 classification map in the North American Land Cover Database (NALCD2005) [27] (Fig. 1). The second study area is an irrigated rice field located in southern New South Wales with an area of 2193 km^2 ([28, Figs. 1(a)–(c)] and Fig. 1). Three clusters were generated by unsupervised classification of the MODIS data, which roughly represent the flood irrigated cropland, furrow irrigated cropland and dryland woodlands, respectively. The MODIS samples were randomly selected according to the classification map.

B. LAI Measurements in Canada Study Area

For the Canada study area, a field campaign for the LAI measurement was performed on August 17-19, 2011. Fourteen 50×50 m^2 plots (Fig. 1) were established by marking two rows of flags. Two of the plots were covered by mixed forest, one by broadleaf forest, and the others by needle forest, which contains black spruce (*Picea mariana*, BS) and jack pine (*Pinus banksiana*, JP) species. There were thirteen sites with trees older than 40 years old, and one site about 20 years old. The effective LAI (L_e) was measured and calculated using the LAI-2000 plant canopy analyzer [29] by using its rings 1–5 (0° to 75°). A foliage clumping index (Ω) characterizing the spatial distribution pattern of the canopy components as a correction factor to obtain the true LAI was used [30]. The clumping index includes two parts: 1) the effect of foliage clumping at scales larger than the shoot, and 2) the needle-to-shoot area ratio quantifying the effect of needles clumping within a shoot. The first part was measured using Tracing Radiation and Architecture of Canopies (TRAC) [31] and the woody-to-total area ratio was set to 0.145, 0.225, and 0.215 for BS, JP, and aspen (*Populus tremuloides*), respectively, while the needle-to-shoot area ratio of 1.57 measured by Chen *et al.* [32] for coniferous forests was used for the second part.

C. Data Preprocessing

For the Canada study area, Landsat 5 TM 1G processing level imagery was collected at three acquisition dates during the growing season of 2009: June 16, September 4, and September 20. The TM images were first radiometrically calibrated and atmospherically corrected using the FLAASH model (Fast Line-of-sight Atmospheric Analysis of Spectral Hypercubes). The aerosol was retrieved using the Kaufman–Tanre (KT) aerosol model [33]. The clouds and cloud shadows were masked out by utilizing an object-based detection algorithm developed by Zhu and Woodcock [34]. For the Australia study area, eight Landsat 7 ETM+ images were collected during the summer growing season (i.e., southern hemisphere) at the following dates: November 25 and December 04 in 2001, and January 05, January 12, February 13, March 10, March 17, and April 2 in 2002, which were preprocessed following Emelyanova *et al.* [28].

For both study areas, the MODIS Nadir BRDF-Adjusted Reflectance (NBAR) products (MODIS/Terra Nadir BRDF-Adjusted Reflectance 16-Day L3 Global 500 m SIN Grid) [35] were collected. Only data with quality label of 'good' were used. The VI derived from MODIS is sensitive to atmospheric effects,

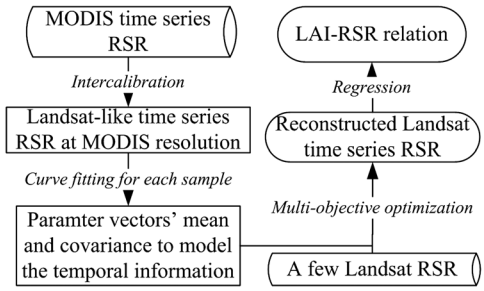

Fig. 2. Flow chart of Landsat RSR time series reconstruction using MODIS time series.

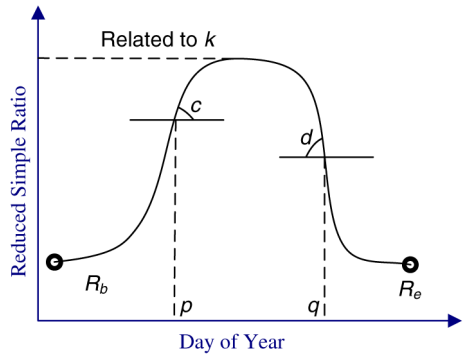

Fig. 3. The seven parameters of the double logistic (D-L) function.

which generally causes a decrease in the retrieved VI. Thus, we first tried to remove such effects using the locally adjusted cubic-spline capping (LACC) data smoothing technique [36]. After data smoothing, some phenological response curves of the MODIS samples may not exhibit a reverse 'U' shape. We eliminated these extraordinary samples first as they may cause bias in retrieving vegetation temporal information. After this elimination, for the Canada study area, a total 792 out of 1000 needle forest samples, 35 out of 40 broadleaf forest samples, and 749 out of 800 mixed forest samples was preserved. For the Australia area, a total 143 out of 200 dryland woodlands samples, 708 out of 800 flood irrigated cropland samples, and 206 out of 300 furrow irrigated cropland samples was preserved.

III. Reconstructing Time Series of Landsat RSR Related to LAI

After data preprocessing, the complex sequence of operations for reconstructing time series of Landsat RSR related to LAI is depicted in the flowchart shown in Fig. 2. Each of the segments is discussed in the rest of this section.

A. Intercalibration of Landsat and MODIS RSR

RSR is an improved version of SR, which is a reflectance ratio between the red and NIR bands,

$$\mathrm{RSR} = \frac{\rho_{\mathrm{NIR}}}{\rho_{\mathrm{red}}}\left[1 - \frac{\rho_{\mathrm{SWIR}} - \min(\rho_{\mathrm{SWIR}})}{\max(\rho_{\mathrm{SWIR}}) - \min(\rho_{\mathrm{SWIR}})}\right] \quad (1)$$

where ρ_{red}, ρ_{NIR}, and ρ_{SWIR} are the red, NIR, and shortwave infrared (SWIR) reflectance, respectively. $\min(\rho_{\mathrm{SWIR}})$ and $\max(\rho_{\mathrm{SWIR}})$ are the minimum and maximum SWIR reflectance after excluding water and shadow pixels. In this study, for Landsat images where all the cloud shadow, cloud, and water pixels have been masked out, they are defined as the 0.4% cutoff points in the histograms of SWIR reflectance in the image. By contrast, for MODIS images, they are defined as the 1% minimum and maximum cutoff points as some pixels in the NBAR composite images are water-mixed due to the large footprint of the MODIS pixel.

Intercalibration was conducted to reduce the RSR difference between Landsat and MODIS sensors [37], [38]. In order to reduce the uncertainties due to the geolocation errors [39] in the intercalibration, both Landsat and MODIS images were degraded to 1.5 km spatial resolution by taking the average of the fine-resolution pixels, which was done for the closest acquisitions available for these two sensors. In the degraded VI maps, we screened out pixels which have more than 10% area affected by the cloud masks of Landsat images, based on which we established a second-order polynomial regression for intercalibration as suggested by Rochdi and Fernandes [40]. All MODIS RSR values were calibrated against the Landsat RSR values by using the established relationship.

B. Modeling Temporal Information Through Fitting D-L Curves

We used the D-L function [21] to express the phenological response curve of RSR, i.e.,

$$R(t) = R_b + \frac{k}{1+\exp[-c(t-p)]} - \frac{k + R_b - R_e}{1+\exp[-d(t-q)]} \quad (2)$$

where t is the time variable (i.e., day of year for the Canada dataset, or day since the start of the growing season for the Australia dataset), R is the RSR and k is related to the maximum value (no dimension) of the RSR during the growing season. The RSR observed before spring green-up differs from that observed at the end of the seasonal cycle (or snow-free observed cycle), which can be represented by R_b and R_e, respectively. c and d (day^{-1}) denote the slopes of the first and second inflection points, respectively, related to the vegetation growing and withering speed. p and q (day) are the dates of the two inflection points. This equation makes ascending and descending parts of the curve non-symmetric, representative for the start and end of the growing season. Physical meanings of the seven parameters are shown in Fig. 3. Given an RSR time series, R_b and R_e can be set to the snow-free RSR at the start and end of the observation period. The other five parameters are fitted through an iterative nonlinear least-squares procedure.

The spectral characteristics of different pixels from the same vegetation type may exhibit a high degree of variability in terms of vegetation species composition, forest structure, vegetation age, and variations in environmental factors (topography, water availability, soil type, etc.) [22], [26]. Thus, they may have different parameter vectors of the fitted D-L curves. All the D-L parameter vectors from vegetation type i are assumed to have a normal distribution as follows:

$$P(i) \sim N(M_i, C_i), \quad P(i), M_i \in R^n \quad C_i \in R^{n\times n} \quad (3)$$

where P represents the parameter vector by stacking the seven D-L parameters in (2) (thus $n = 7$, $P = [c\ p\ d\ q\ k\ R_b\ R_e]^T$), and M_i and C_i are the mean vector and covariance matrix of the parameter vectors, respectively.

Mixed pixels are more frequent and pure pixels are fewer in MODIS images than in their corresponding Landsat images. However, to blend these two types of images we assume that pixels from the same vegetation type in different spatial resolutions may share similar combination of possible pixel types (each pixel type has a specific vegetation species combination, vegetation age, vegetation density, and environmental condition). Hence, the D-L parameter vectors for all the RSR time series derived from Landsat data follow the same distribution derived from the MODIS data as depicted in (3).

C. Reconstructing Time Series of Landsat RSR Through Multi-Objective Optimization

The time series of the Landsat RSR is reconstructed through an optimization to achieve two objectives. The first objective, F_1, is that the fitted curve should be as close as possible to the observed Landsat RSR. Given a Landsat sample x, suppose $t = 1, 2, \ldots, N$ is a set of the Landsat acquisition dates with observed value of RSR_t,

$$F_1 = \sum_{t=1}^{N} (dl(t, P_x) - RSR_t)^2 / N \tag{4}$$

where $dl(t, P_x)$ is the D-L function with parameter vector P_x. The second objective, F_2, is that the derived D-L parameters should follow the normal distribution (Eq. (3)). Suppose the target Landsat pixel x belongs to a vegetation type i,

$$F_2 = (P_x - M_i)^T C_i^{-1} (P_x - M_i). \tag{5}$$

The parameter vector P_x should also satisfy three constraints. First, k and ($k + R_b$-R_e) should be greater than 0, which is the necessary condition to make RSR increase at the start and decrease at the end of the growing season. Second, R_b and R_e should be greater than 0. Third, P_x should be in the range of ± 2 standard deviations.

The main uncertainty of the first objective comes from the observed Landsat RSR, e.g., bias in radiometric calibration, sensor system noise, or imprecise parameters used in the atmospheric correction [4], and it should not vary much among different cover types. Thus, the first objective in (4) utilizes an identity covariance matrix unlike the specific covariance matrix as a function of land cover class as specified in (5) for the second objective. It should be noted that the two objectives serving for different purposes and bearing different units are complimentary and competitive. They are treated in the same dimension in optimization because their values are both normalized: the first objective represents a normalized distance of RSR, while the second represents a normalized deviation measure of parameter values. To measure and reflect the relative uncertainty (covariance matrix) of the constraint given by objective 1 versus objective 2, a relative scaling parameter w is introduced. Then by minimizing the maximum of $[wF_1, F_2]$, the optimal parameter vector P_x^* can be obtained by solving the following optimization problem with inequality constraints, i.e.,

$$\begin{aligned} \min \quad & f(P_x) = \min \quad [\max(wF_1(P_x), F_2(P_x))] \\ \text{s.t.} \quad & M - 2diag(C) \le P_x \le M + 2diag(C) \\ & k > 0, \quad k + R_b - R_e > 0, \quad R_b > 0, \quad R_e > 0 \end{aligned} \tag{6}$$

where $diag$ extracts the diagonal of an array. We used the Matlab Optimization Toolbox to solve such an equation, where a maximum number of 400 iterations and the termination tolerance on the function value of 1E-6 are set.

The proposed method is vegetation-type-based. Given a Landsat pixel without its cover type information, we selected a model from the three vegetation type models whose mean RSR has the shortest Euclidean distance to the observed Landsat RSR as presumably related to this vegetation type.

The absolute difference (AD), relative difference (RD), correlation coefficient (CC), and root mean square error (RMSE) were used as the assessment criteria for evaluation. AD is defined as the absolute difference between the reconstructed and the observed RSR. RD is defined as the ratio of AD to the observed value. CC, known as Pearson's R, is a measure of the strength of the linear relationship between the reconstructed and the observed RSR. The method proposed by Gray and Song (GS) has been used for comparison. Note the necessary condition of their method, that two Landsat observations should be acquired when VI is at its minima and maxima, is mostly not satisfied in our observation date combination set. We thus extend their method by using objective 1 in (4) to estimate R_b, R_e, and k, where $R_b = R_e$, while the other four parameters of the D-L curve are set to their mean value as done by Gray and Song [24].

D. Developing Relationship between RSR and LAI

There exists a linear regression relationship between RSR and LAI, i.e.,

$$RSR = \alpha LAI + \beta. \tag{7}$$

It should be noted that such a relationship may vary both seasonally in response to phenological development of the trees and solar zenith angle variations of the observation data.

IV. Experimental Results

A. MODIS RSR Fitted With D-L Function

Table I shows the average RMSE for all samples in each vegetation type for the Canada study area. For all the three vegetation types, the RMSE was smaller than 0.15. The mean (M) and standard deviation (SD) (the diagonal element in the covariance matrix) of the fitted parameter vectors are shown in Table II. Without exception, the three parameters R_b, c, and p, representing the starting growing season, always had lower SDs than their corresponding parameters R_e, d, and q representing the end of the growing season. A possible explanation is that, at the end of the growing season, the variation caused by environmental factors accumulated from the start of the growing

season and thus the spectral characteristic differences among pixels were larger than those at the start of the growing season.

B. Validation Against MODIS RSR

The MODIS seasonal VI time series was first reconstructed from their RSR values acquired at only a few dates (less than or equal to 7) by using the Canada forest study area. Then the MODIS RSR values observed on the other dates were used for the validation. Two sets (A and B) of observation dates combination were used for the reconstruction based on their distribution pattern. The observation dates in the set A were *equally* distributed along the observation period and have different numbers of MODIS observations from 2 to 7 on the following dates: [185 265], [153 217 281], [145 193 221 289], [137 177 217 257 297], [129 169 201 233 265 305], and [129 161 193 217 249 281 313]. The dates in the set B were *randomly* distributed along the observation period and have [121 281], [209 217 249], [209 273 281 289], [185 217 241 249 281], [129 161 257 265 273 289], and [121 129 161 177 273 281 289]. The average AD and average RD were calculated for each vegetation type as functions of the number of MODIS observations in set A (Fig. 4). Mostly, the proposed method was superior to the GS method. For the proposed method, 1) the average ADs among these three types had some differences (Fig. 4(a)), while as for the average RDs there were no large differences among them (Fig. 4(b)) due to the differences in the original RSR values; 2) as the number of observation dates increased, the error decreased. For GS method, 1) the accuracy was sensitive to the forest type and was superior for the broadleaf forest; 2) increasing the number of the observation dates contributed little to the reconstruction accuracy. In the following experiments of this section, if not specified the relative scaling parameter w was set to 10.

The sensitivity analysis of the relative scaling parameter w in (6) for the two MODIS experimental sets was performed (Fig. 4). A larger value of w means more contribution from the first objective and the less contribution from the second objective. An extreme case would be that w is infinity, where only the first objective is effective in the optimization. In such a case, it is the same as the GS method except that seven D-L parameters are to be estimated (only two in GS). Obviously, it is an ill-posed problem as we do not have seven Landsat observations for the estimation. The randomness and the dependence on the initial value of the solution will be high from the mathematical perspective, while there may be many curves satisfying the minimization of the first objective. In all the experiments, the initial values were set to be the mean parameters as specified in Table II. We draw such case (Fig. 4) as w is 'INF'. Too much contribution from objective 2 may restrict the solution space to a small interval around the mean value, which may not contain the best solution. Thus, for all the cases the accuracy increased with increasing w when it was less than 5 (Fig. 4). Too small contribution from objective 2 may not properly restrict the solution in the right interval. Thus, for w values greater than 20, the accuracy decreased for some date combinations, especially for the set B experiment (Fig. 4(d)), indicating the contribution of the second objective. The accuracy was stable and best when w ranged from 5 to 20, which did not vary among different cover types. An interesting finding was that when w equals to infinity, the reconstruction accuracy from six MODIS observations was much worse than that from five or even fewer observations (Fig. 4 (d), (f), and (h)). This is because without the second objective to constrain the curve towards a regular seasonal pattern, the more observations used for the reconstruction, the higher tendency to over-fitting of the observed values. The over-fitting happened even when we had seven observations (enough to estimate unknown parameters) for the reconstruction (Fig. 4 (d), (f), and (h)). Such cases also indicated the importance of the second objective.

Comparing sets A and B in Fig. 4, we can see that the distribution of the acquisition dates did affect the reconstructed result. We used three MODIS observations for the reconstruction but with 13 different acquisition date combinations which were randomly distributed (Fig. 5). As expected, the more spread out is the distribution of the acquisition dates, the higher the reconstruction accuracy.

TABLE I
RMSE OF FITTED CURVES FOR THREE VEGETATION TYPES

Vegetation type	Needle	Broadleaf	Mixed
Samples	792	35	749
Average RMSE	0.1378	0.0778	0.1087

TABLE II
MEAN (M) AND STANDARD DEVIATION (SD) OF ALL THE PARAMETERS RETRIEVED FROM EACH VEGETATION TYPE

		R_b	R_e	k	c	d	p	q
N	M	4.51	5.31	2.61	-0.06	-0.05	175	275
	SD	0.61	0.84	5.49	0.036	0.07	25.5	39.7
B	M	2.75	2.63	1.36	-0.06	-0.05	163	265
	SD	0.38	0.39	5.63	0.04	0.16	26.1	25.3
M	M	3.63	3.75	2.16	-0.06	-0.06	161	270
	SD	0.55	0.75	5.01	0.03	0.02	25.6	28.9

In the first column, 'N' indicates needle forest with 792 samples, 'B' indicates broadleaf forest with 35 samples, and 'M' indicates mixed forest with 749 samples.

C. Validation Against Landsat RSR

There are still some non-vegetation (e.g., bare land) pixels in the Landsat images after masking out water and cloud pixels. The rules for building vegetation masks were that for the Canada forest area the vegetation pixels should have RSR values greater than 3.0 on September 4 and for the Australia cropland study area the average vegetation pixel RSR of the eight Landsat images should be greater than 1.0.

For the Canada forest area, TM observations at two of the three acquisition dates in 2009 are used for the reconstruction and the remaining one is used for the validation. If two TM observations on June 16 and September 20 are used for the reconstruction, the observed TM data on September 4 will be used for the validation. We refer to this case as 'September 4' validation experiment. Similarly 'June 16' and 'September 20' validation experiments are also defined. For the Australia cropland area, with eight Landsat images available, reconstruction was made

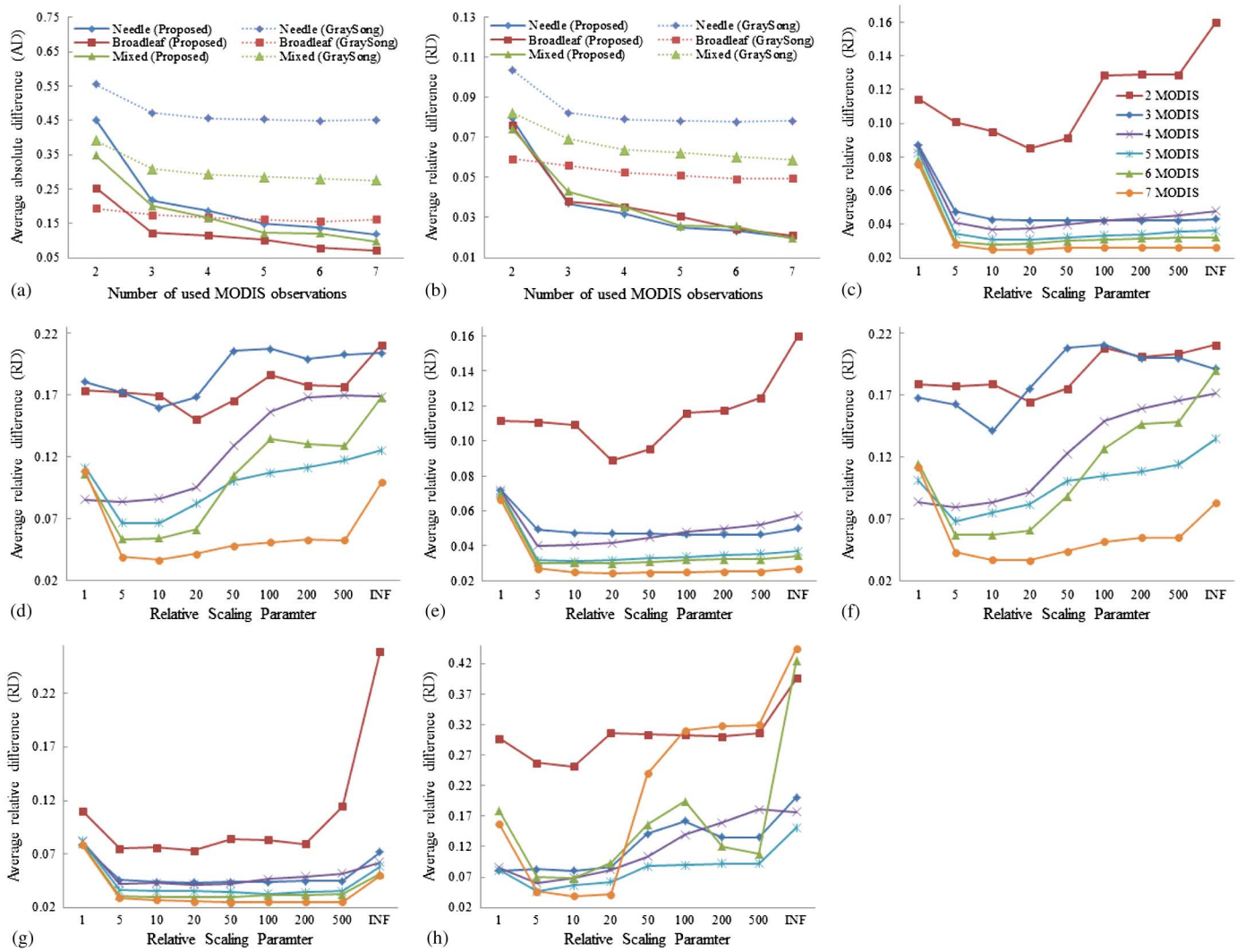

Fig. 4. The average AD (a) and average RD (b) as functions of the number of MODIS observations used in the reconstruction for set A by using different methods for different vegetation types. The average AD as functions of the relative scaling parameter w for MODIS sets A and B for needle forest (c) and (d), mixed forest (e) and (f) and broadleaf forest (g) and (h). The legends for (c)–(h) are all the same as shown in (c).

using 2 to 7 Landsat images which results in the following image combinations: [4 6], [2 4 6 8], [1 2 4 6 8], [1 2 4 5 6 8], and [1 3 4 5 6 7 8]. These combinations were chosen because their distributions are relatively spread in the whole observation period. Another experiment by using the seven Landsat images (which are enough to estimate the seven unknown D-L parameters) for reconstruction was designed without using the second objective, which was referred to as the 'INF' case. The relative scale parameter was set to 5 for all the following experiments.

Figs. 6–9 show the comparison between the reconstructed RSR and the observed Landsat RSR in different ways. These two kinds of RSR maps were quite consistent (Fig. 6). The reconstructed RSR map can be used to replace the affected pixels (Fig. 6(b) and (c)). Comparing the three experiments for the Canada forest area, the worst reconstructed results were found in the 'June 16' validation experiment (Fig. 7). This is because in that experiment, RSRs observed at both dates for the reconstruction were within the end of the growing period and thus provided little information for the start of the growing period.

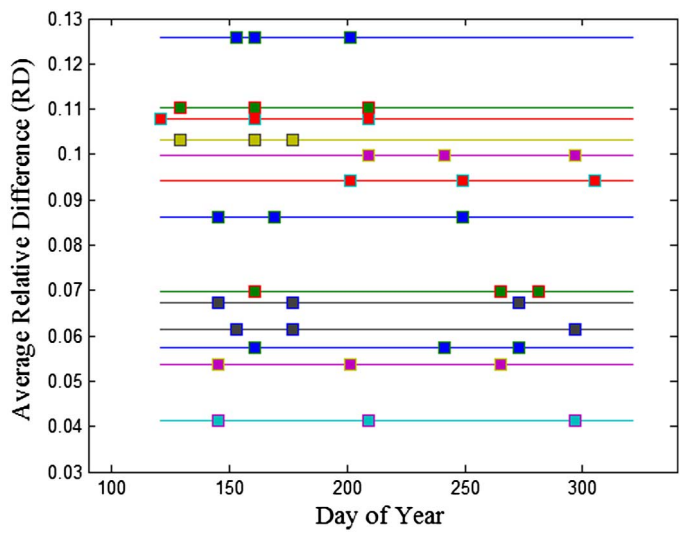

Fig. 5. Reconstruction accuracy sensitivity to acquisition date combinations (the rectangles by different colors) (each line represents its corresponding accuracy) for reconstruction.

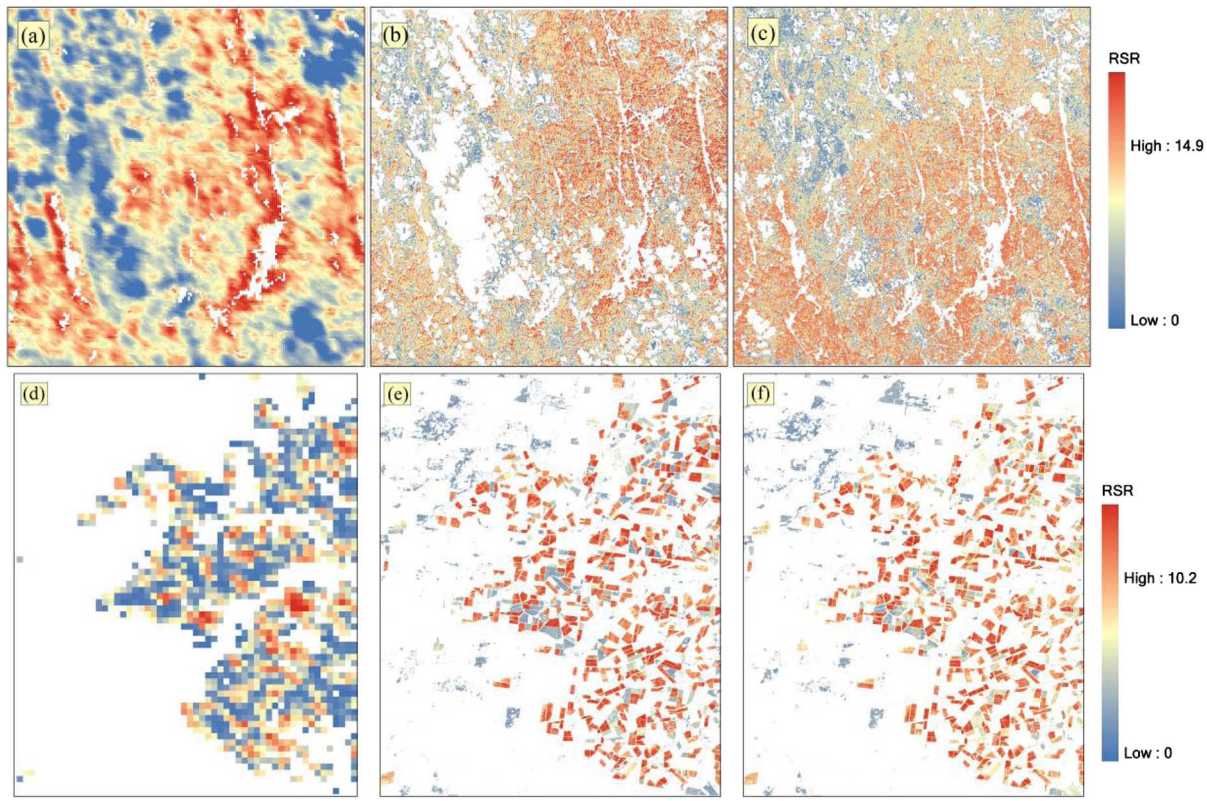

Fig. 6. (Top) The MODIS RSR image (after calibration) from the NBAR August 29–September 13 composite (a), the TM RSR images observed on September 4 (b), reconstructed on September 4 from two Landsat images (c) for the Canada forest area; and (Bottom) The MODIS RSR image (after calibration) from the NBAR December 27, 2001–January 11, 2002 composite (d), the ETM+ RSR images observed (e) on January 5, 2002, and reconstructed (f) on January 5, 2002 from the other seven images for the Australia cropland area. The non-vegetation pixels are displayed as white.

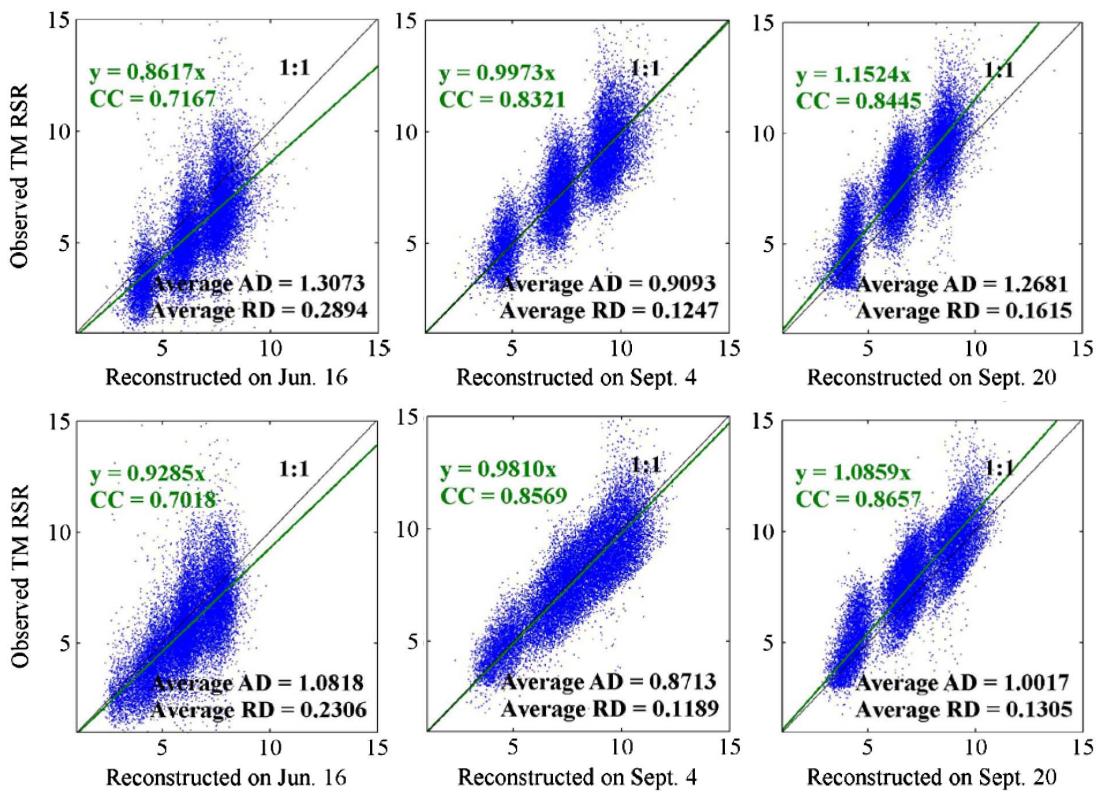

Fig. 7. The observed RSR against the reconstructed RSR from both the GS method (top) and the proposed method (bottom) for the three validation experiments for the Canada forest area, where CC is correlation coefficient, AD is absolute difference, and RD is relative difference.

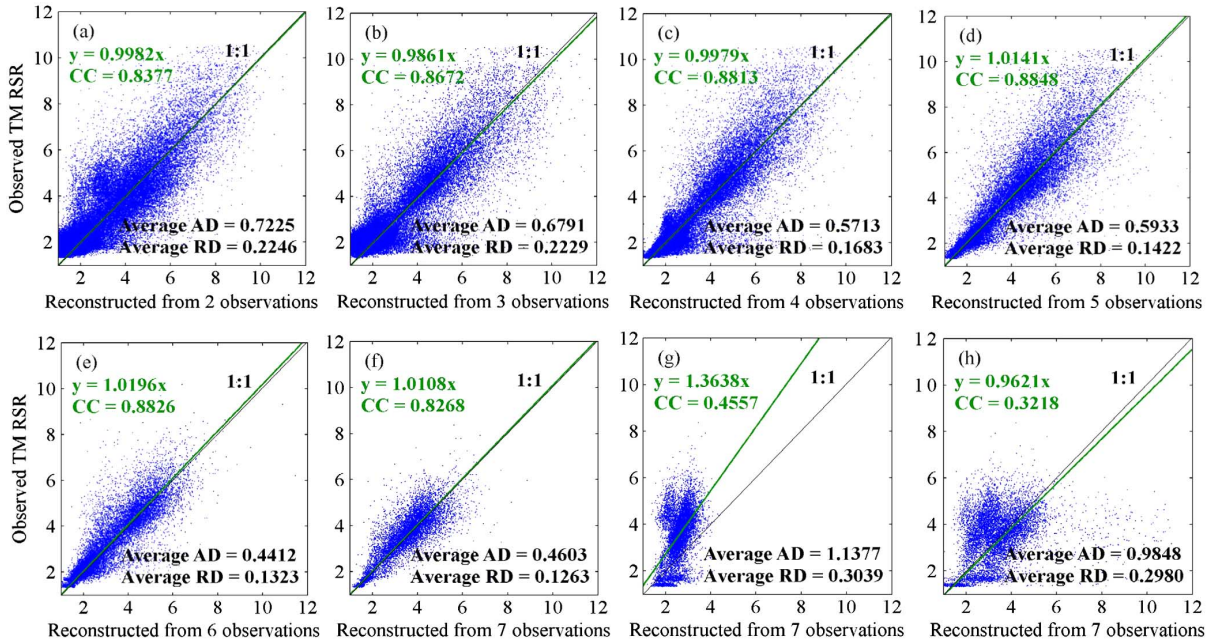

Fig. 8. The observed versus the reconstructed Landsat RSR from the proposed method for the six validation experiments (a)–(f), the GS method (g) and INF method (h) using seven Landsat images for the Australia cropland area, where CC is correlation coefficient, AD is absolute difference, and RD is relative difference.

The reconstructed results by the GS method showed its weakness compared to that by the proposed method (Fig. 7) as the GS method allowed changing only R_b and R_e in the optimization, which was more obvious when the number of TM observations used for the reconstruction was larger than two (e.g., seven in Fig. 8(f) and (g)). The more Landsat images used for the reconstruction, the better accuracy (RD and AD in Fig. 8) could be achieved. Comparing Fig. 8(f) with Fig. 8(h), the contribution of the second objective was obvious even though we had seven Landsat images for the reconstruction. These findings corresponded to the experimental results from the MODIS dataset in Section IV-B.

D. Utility for the Development of the Relationship Between LAI and RSR

For the Canada study area, the LAI measurement date was different from any of the TM acquisition dates (Fig. 9(d)). Thus, we used the RSR on the LAI measurement date reconstructed from all three TM acquisitions for the relationship development. The effective LAI values were plotted against the reconstructed RSR on the LAI measurement date (August 18, 2009, Fig. 10(d)) and the observed TM RSR acquired at the three different dates (Fig. 10(a)–(c)). Correspondingly, the true LAI values were also plotted against different kinds of RSR (Fig. 11). The trend line in each plot was fitted by using (7) with β value of 0 (Figs. 10 and 11), which represented the offset in the linear relationship.

Comparing Figs. 10 and 11(a)–(c), the correlation (R square) between effective (true) LAI and the TM RSR acquired on June 16 was better than that on September 4 and September 20. The poor performance on September 4 was possibly because four of the 14 plots were very close (three of them are less than 50 m) to the cloud pixels that day. However, the poor performance on September 20 may be because that interval between August 20 and September 20 was at the end of the growing season which showed more seasonal variation than between June 16 and August 18, at the start of the growing season (Table II).

Comparing Figs. 10, 11(d) with Figs. 10, 11(a)–(c), the reconstructed RSR on the LAI measurement date had better relationships (higher R squares) with the effective (true) LAI than the observed Landsat RSR on the three acquisition dates. This indicated that the temporal information borrowed from the time series of MODIS RSR could help reconstruct the RSR seasonal variation at Landsat resolution by the proposed method.

The regression significance between RSR and the effective LAI was greater than that with the true LAI. This was similar to the results in [3] regarding relationships between SR and LAI. This is because the essential optical remote sensing signal is from the canopy and its gap fraction, which is converted to effective LAI rather than LAI. Mono-angle remote sensing such as Landsat TM is more sensitive to effective LAI than to true LAI with clumping [41].

The α coefficients, which represented the slopes in the linear relationships between the true LAI and the RSR observed on June 16, September 4, and September 20 shown in Fig. 11(a)–(c), were closer to 1.242 in [13] than that between true LAI and the reconstructed RSR on August 18, as they both have a mismatch between the acquisition dates of satellite data and the LAI measurement date due to the difficulty of collecting Landsat data as stated in Section I.

V. Conclusion

This paper presents a novel spatiotemporal fusion algorithm based on the D-L function and a multi-objective optimization method to reconstruct seasonal variation of RSR at high spatial resolution. The experiments of reconstructing RSR time series

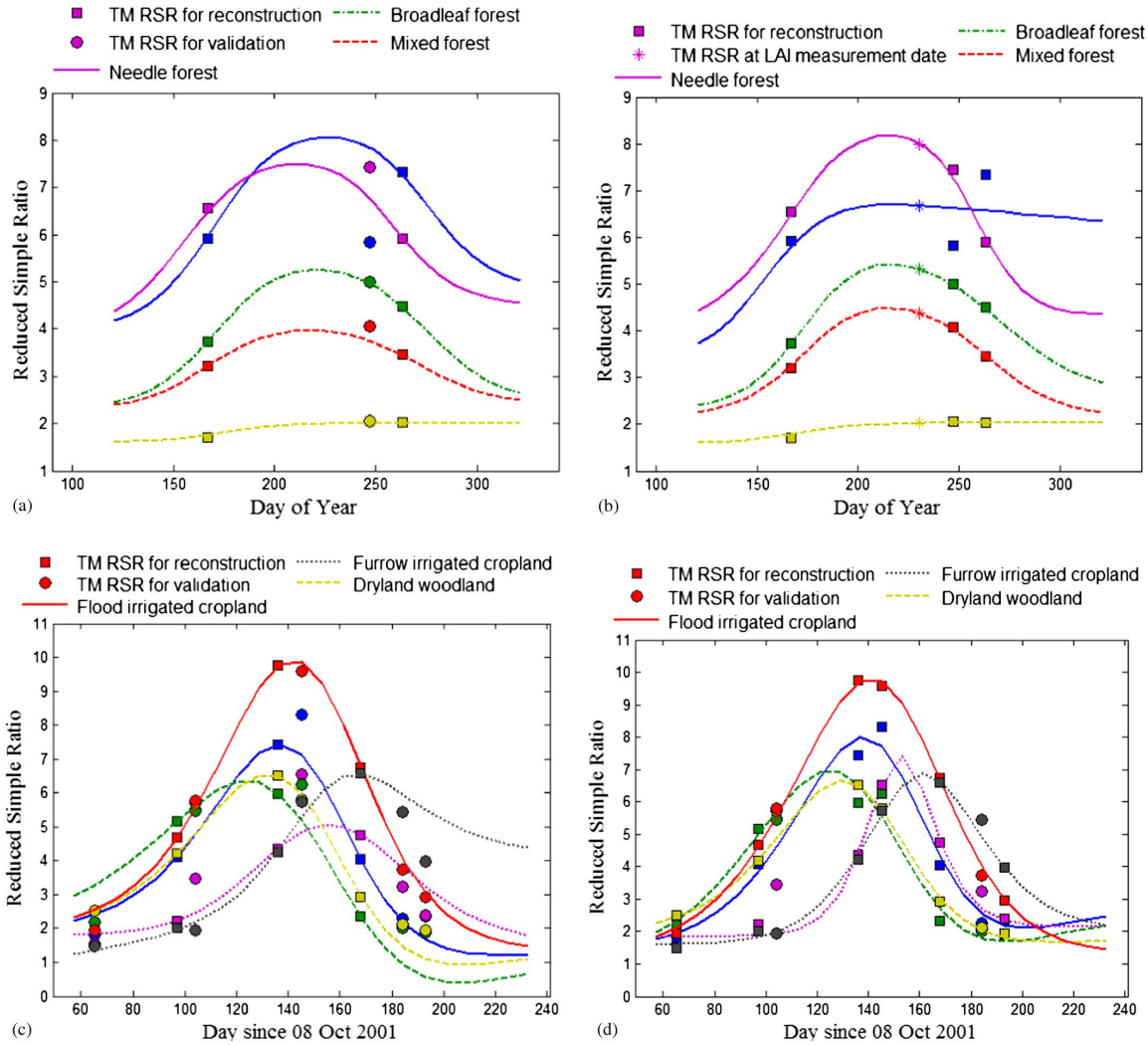

Fig. 9. The reconstructed RSR time series of five (two needle forest, two mixed forest, and one broadleaf forest) samples selected from the 14 LAI measurement plots in the Canada study area (a) and (b), and the reconstructed RSR time series of six (two dryland woodlands, two flood irrigated cropland, and two furrow irrigated cropland) samples selected in the Australia study area (c) and (d). The TM RSR for the reconstruction (squares), TM RSR for the validation (circles), reconstructed TM RSR on the LAI measurement date (stars), and the reconstructed time series RSR for each sample (lines) are represented by a unique color. (a) September 4 validation experiment. (b) Reconstructed time series from the observed RSR on the three acquisition dates. (c) Reconstructed from three observations. (d) Reconstructed from six observations.

at the Landsat resolution were conducted on a Canada boreal forest and an Australia cropland area. The more Landsat observations are used for the reconstruction, the better accuracy can be achieved. The MODIS prior constraint to the reconstruction made it possible to estimate the seven D-L parameters without using seven or more Landsat images. It can avoid the over-fitting problem when even only seven or a few more than seven Landsat images were used for the reconstruction. The reconstructed RSR was plotted against the LAI, which showed a better relationship than the observed RSR at dates which differ from the LAI measurement date, indicating the temporal information from MODIS time series data was well-blended into the Landsat data.

Although the proposed method is applied to RSR in this study, it can also be used to reconstruct seasonal variation of surface reflectance in individual bands. One aspect that we would like to explore in the future is to validate seasonal LAI and phenology parameters (e.g., onset and dormancy dates) derived from the proposed method against ground observations.

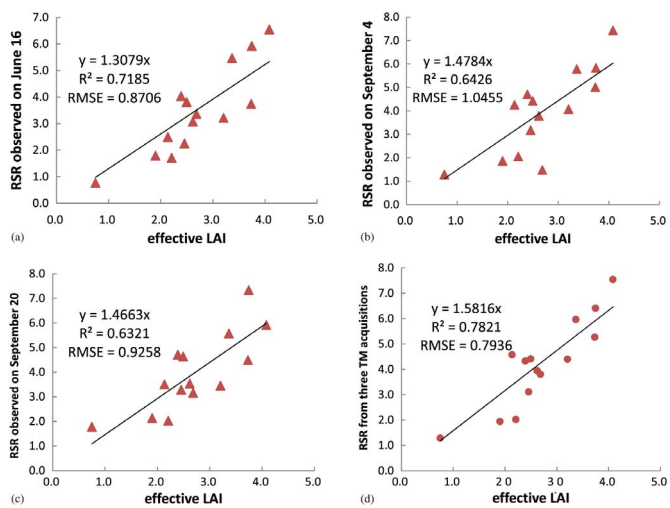

Fig. 10. Linear regression models between effective LAI and RSR (observed RSR acquired (a) on June 16, (b) on September 4, and (c) on September 20, and (d) reconstructed RSR on August 18 from the three TM acquisitions).

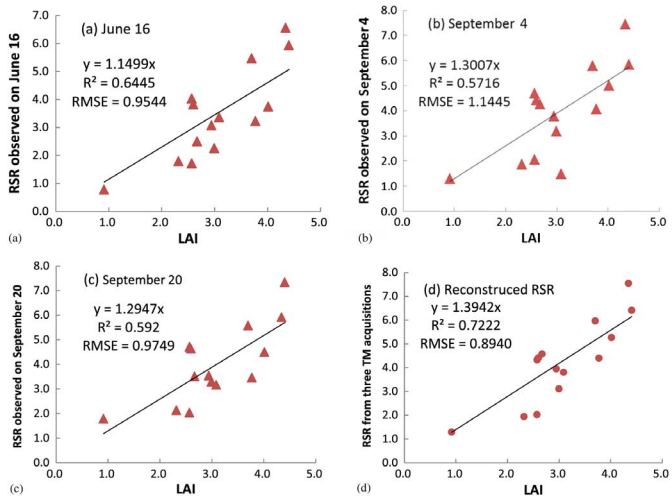

Fig. 11. Linear regression models between true LAI and RSR (observed RSR acquired (a) on June 16, (b) on September 4, and (c) on September 20, and (d) reconstructed RSR on August 18 from the three TM acquisitions).

ACKNOWLEDGMENT

The first author would like to thank The Chinese University of Hong Kong (CUHK) for supporting him to visit the University of Toronto under the Ph.D. Student Exchange Programme 2011–12. The authors would like to thank Peter Czurylowicz for helping them to perform the field campaign near Sudbury, Canada. Special thanks are due to Dr. Gonsamo Alemu for his valuable comments on the subject of the paper.

REFERENCES

[1] J. M. Chen and T. A. Black, "Defining leaf area index for non-flat leaves," *Plant, Cell Environ.*, vol. 15, no. 4, pp. 421–429, 1992.

[2] T. N. Carlson and D. A. Ripley, "On the relation between NDVI, fractional vegetation cover, and leaf area index," *Remote Sens. Environ.*, vol. 62, no. 3, pp. 241–252, 1997.

[3] J. M. Chen and J. Cihlar, "Retrieving leaf area index of boreal conifer forests using Landsat TM images," *Remote Sens. Environ.*, vol. 55, no. 2, pp. 153–162, 1996.

[4] C. R. Butson and R. A. Fernandes, "A consistency analysis of surface reflectance and leaf area index retrieval from overlapping clear-sky Landsat ETM+ imagery," *Remote Sens. Environ.*, vol. 89, no. 3, pp. 369–380, 2004.

[5] L. Brown, J. M. Chen, S. G. Leblanc, and J. Cihlar, "A shortwave infrared modification to the simple ratio for LAI retrieval in boreal forests: An image and model analysis," *Remote Sens. Environ.*, vol. 71, no. 1, pp. 16–25, 2000.

[6] L. Eklundh, K. Hall, H. Eriksson, J. Ardo, and P. Pilesjo, "Investigating the use of Landsat thematic mapper data for estimation of forest leaf area index in southern sweden," *Can. J. Remote Sens.*, vol. 29, no. 3, pp. 349–362, Jun. 2003.

[7] P. Stenberg, M. Rautiainen, T. Manninen, P. Voipio, and H. Smolander, "Reduced simple ratio better than NDVI for estimating LAI in Finnish pine and spruce stands," *Silva Fenn.*, vol. 38, no. 1, pp. 3–14, 2004.

[8] P. Stenberg, M. Rautiainen, T. Manninen, P. Voipio, and M. Mottus, "Boreal forest leaf area index from optical satellite images: Model simulations and empirical analyses using data from central Finland," *Boreal Environ. Res.*, vol. 13, pp. 433–443, Oct. 2008.

[9] Y. Wang, C. E. Woodcock, W. Buermann, P. Stenberg, P. Voipio, H. Smolander, T. Häme, Y. Tian, J. Hu, Y. Knyazikhin, and R. B. Myneni, "Evaluation of the MODIS LAI algorithm at a coniferous forest site in Finland," *Remote Sens. Environ.*, vol. 91, no. 1, pp. 114–127, 2004.

[10] X. Chen, L. Vierling, D. Deering, and A. Conley, "Monitoring boreal forest leaf area index across a siberian burn chronosequence: A MODIS validation study," *Int. J. Remote Sens.*, vol. 26, no. 24, pp. 5433–5451, 2005.

[11] Q. Tian, Z. Luo, J. M. Chen, M. Chen, and F. Hui, "Retrieving leaf area index for coniferous forest in Xingguo County, China with Landsat ETM+ images," *J. Environ. Manag.*, vol. 85, no. 3, pp. 624–627, 2007.

[12] J. Heiskanen, M. Rautiainen, L. Korhonen, M. Mõttus, and P. Stenberg, "Retrieval of boreal forest LAI using a forest reflectance model and empirical regressions," *Int. J. Appl. Earth Observ.*, vol. 13, no. 4, pp. 595–606, 2011.

[13] J. M. Chen, G. Pavlic, L. Brown, J. Cihlar, S. G. Leblanc, H. P. White, R. J. Hall, D. R. Peddle, D. J. King, J. A. Trofymow, E. Swift, J. Van der Sanden, and P. K. E. Pellikka, "Derivation and validation of Canada-wide coarse-resolution leaf area index maps using high-resolution satellite imagery and ground measurements," *Remote Sens. Environ.*, vol. 80, no. 1, pp. 165–184, Apr. 2002.

[14] D. Huang, W. Z. Yang, B. Tan, M. Rautiainen, P. Zhang, J. N. Hu, N. V. Shabanov, S. Linder, Y. Knyazikhin, and R. B. Myneni, "The importance of measurement errors for deriving accurate reference leaf area index maps for validation of moderate-resolution satellite LAI products," *IEEE Trans. Geosci. Remote Sens.*, vol. 44, no. 7, pp. 1866–1871, Jul. 2006.

[15] F. Deng, J. M. Chen, S. Plummer, M. Chen, and J. Pisek, "Algorithm for global leaf area index retrieval using satellite imagery," *IEEE Trans. Geosci. Remote Sens.*, vol. 44, no. 8, pp. 2219–2229, 2006.

[16] S. Garrigues, D. Allard, F. Baret, and M. Weiss, "Influence of landscape spatial heterogeneity on the non-linear estimation of leaf area index from moderate spatial resolution remote sensing data," *Remote Sens. Environ.*, vol. 105, no. 4, pp. 286–298, Dec. 2006.

[17] J. M. Chen, "Spatial scaling of a remotely sensed surface parameter by contexture," *Remote Sens. Environ.*, vol. 69, no. 1, pp. 30–42, Jul. 1999.

[18] B. Huang, H. K. Zhang, and L. Yu, "Improving Landsat ETM plus urban area mapping via spatial and angular fusion with MISR multi-angle observations," *IEEE J. Sel. Topics Appl. Earth Observ. Remote Sens. (JSTARS)*, vol. 5, no. 1, pp. 101–109, 2012.

[19] F. Gao, J. Masek, M. Schwaller, and F. Hall, "On the blending of the Landsat and MODIS surface reflectance: Predicting daily Landsat surface reflectance," *IEEE Trans. Geosci. Remote Sens.*, vol. 44, no. 8, pp. 2207–2218, Aug. 2006.

[20] B. Huang and H. Song, "Spatiotemporal reflectance fusion via sparse representation," *IEEE Trans. Geosci. Remote Sens.*, vol. 50, no. 10, pp. 3707–3716, 2012.

[21] A. Fischer, "A model for the seasonal-variations of vegetation indexes in coarse resolution data and its inversion to extract crop parameters," *Remote Sens. Environ.*, vol. 48, no. 2, pp. 220–230, May 1994.

[22] J. I. Fisher, J. F. Mustard, and M. A. Vadeboncoeur, "Green leaf phenology at landsat resolution: Scaling from the field to the satellite," *Remote Sens. Environ.*, vol. 100, no. 2, pp. 265–279, Jan. 2006.

[23] P. S. A. Beck, C. Atzberger, K. A. Hogda, B. Johansen, and A. K. Skidmore, "Improved monitoring of vegetation dynamics at very high latitudes: A new method using MODIS NDVI," *Remote Sens. Environ.*, vol. 100, no. 3, pp. 321–334, Feb. 15, 2006.

[24] J. Gray and C. H. Song, "Mapping leaf area index using spatial, spectral, and temporal information from multiple sensors," *Remote Sens. Environ.*, vol. 119, no. 4, pp. 173–183, Apr. 2012.

[25] Y. Dong, J. Wang, C. Li, G. Yang, Q. Wang, F. Liu, J. Zhao, H. Wang, and W. Huang, "Comparison and analysis of data assimilation algorithms for predicting the leaf area index of crop canopies," *IEEE J. Sel. Topics Appl. Earth Observ. Remote Sens. (JSTARS)*, vol. 6, no. 1, pp. 188–201, 2013.

[26] M. A. White and R. R. Nemani, "Real-time monitoring and short-term forecasting of land surface phenology," *Remote Sens. Environ.*, vol. 104, no. 1, pp. 43–49, Sep. 2006.

[27] North American Land Cover at 250 m spatial resolution, Produced by Natural Resources Canada/Canadian Centre for Remote Sensing (NRCan/CCRS), United States Geological Survey (USGS); Insituto Nacional de Estadística y Geografía (INEGI), Comisión Nacional para el Conocimiento y Uso de la Biodiversidad (CONABIO) and Comisión Nacional Forestal (CONAFOR), NALC, 2005.

[28] I. V. Emelyanova, T. R. McVicar, T. G. Van Niel, L. T. Li, and A. I. J. M. van Dijk, "Assessing the accuracy of blending Landsat–MODIS surface reflectances in two landscapes with contrasting spatial and temporal dynamics: A framework for algorithm selection," *Remote Sens. Environ.*, vol. 133, pp. 193–209, 2013.

[29] *LAI-2000 Plant Canopy Analyzer Operating Manual*, LI-COR Inc., Lincoln, NE, USA, Apr. 1992.
[30] J. M. Chen, J. Liu, S. G. Leblanc, R. Lacaze, and J.-L. Roujean, "Multi-angular optical remote sensing for assessing vegetation structure and carbon absorption," *Remote Sens. Environ.*, vol. 84, no. 4, pp. 516–525, 2003.
[31] J. M. Chen and J. Cihlar, "Plant canopy gap-size analysis theory for improving optical measurements of leaf-area index," *Appl. Opt.*, vol. 34, no. 27, pp. 6211–6222, 1995.
[32] J. M. Chen, A. Govind, O. Sonnentag, Y. Q. Zhang, A. Barr, and B. Amiro, "Leaf area index measurements at Fluxnet-Canada forest sites," *Agricult. For. Meteorol.*, vol. 140, no. 1-4, pp. 257–268, Nov. 2006.
[33] Y. J. Kaufman, A. E. Wald, L. A. Remer, B. C. Gao, R. R. Li, and L. Flynn, "The MODIS 2.1-μm channel-correlation with visible reflectance for use in remote sensing of aerosol," *IEEE Trans. Geosci. Remote Sens.*, vol. 35, no. 5, pp. 1286–1298, Sep. 1997.
[34] Z. Zhu and C. E. Woodcock, "Object-based cloud and cloud shadow detection in Landsat imagery," *Remote Sens. Environ.*, vol. 118, no. 3, pp. 83–94, Mar. 2012.
[35] B. Schaaf, F. Gao, A. H. Strahler, W. Lucht, X. W. Li, T. Tsang, N. C. Strugnell, X. Y. Zhang, Y. F. Jin, J. P. Muller, P. Lewis, M. Barnsley, P. Hobson, M. Disney, G. Roberts, M. Dunderdale, C. Doll, R. P. d'Entremont, B. X. Hu, S. L. Liang, J. L. Privette, and D. Roy, "First operational BRDF, albedo nadir reflectance products from MODIS," *Remote Sens. Environ.*, vol. 83, no. 1-2, pp. 135–148, Nov. 2002.
[36] J. M. Chen, F. Deng, and M. Z. Chen, "Locally adjusted cubic-spline capping for reconstructing seasonal trajectories of a satellite-derived surface parameter," *IEEE Trans. Geosci. Remote Sens.*, vol. 44, no. 8, pp. 2230–2238, Aug. 2006.
[37] M. D. Steven, T. J. Malthus, F. Baret, H. Xu, and M. J. Chopping, "Intercalibration of vegetation indices from different sensor systems," *Remote Sens. Environ.*, vol. 88, no. 4, pp. 412–422, Dec. 2003.
[38] H. Zhang and B. Huang, "Support vector regression-based downscaling for intercalibration of multiresolution satellite images," *IEEE Trans. Geosci. Remote Sens.*, vol. 51, no. 3, pp. 1114–1123, Mar. 2013.
[39] B. Tan, C. E. Woodcock, J. Hu, P. Zhang, M. Ozdogan, D. Huang, W. Yang, Y. Knyazikhin, and R. B. Myneni, "The impact of gridding artifacts on the local spatial properties of MODIS data: Implications for validation, compositing, and band-to-band registration across resolutions," *Remote Sens. Environ.*, vol. 105, no. 2, pp. 98–114, Nov. 30, 2006.
[40] N. Rochdi and R. Fernandes, *Intercalibration of Vegetation Indices from Landsat ETM+ and MODIS 500m Data for LAI Mapping.* Ontario, Canada: Geomatics Canada, 2008, Technical Note 3.
[41] J. M. Chen, C. H. Menges, and S. G. Leblanc, "Global mapping of foliage clumping index using multi-angular satellite data," *Remote Sens. Environ.*, vol. 97, no. 4, pp. 447–457, Sep. 2005.

Hankui Zhang received the B.S. degree in geographic information systems and the M.S. degree in remote sensing from Zhejiang University, Hangzhou, China, in 2007 and 2010, respectively, and the Ph.D. degree in geography and resource management from the Chinese University of Hong Kong, Hong Kong, in 2013.

Currently, he is a Postdoctoral Fellow with the Chinese University of Hong Kong. His research interests are in the remote sensing image fusion and geometric processing of high-resolution satellite images.

Jing M. Chen received the B.Sc. degree in applied meteorology from the Nanjing Institute of Meteorology, Nanjing, China, in 1982, and the Ph.D. degree in meteorology from Reading University, Reading, U.K., in 1986.

From 1989 to 1993, he was a Postdoctoral Fellow and Research Associate with the University of British Columbia, Vancouver, BC, Canada. From 1993 to 2000, he was a Research Scientist with the Canada Center for Remote Sensing, Ottawa, ON, Canada. Currently, he is a Professor with the University of Toronto, Toronto, ON, Canada, and an Adjunct Professor with York University, Toronto. He has published over 200 papers in refereed journals. His recent research interests are in the remote sensing of biophysical parameters, plant canopy radiation modeling, terrestrial water and carbon cycle modeling, and atmospheric inverse modeling for global and regional carbon budget estimation.

Dr. Chen is a Fellow of the Royal Society of Canada and a Senior Canada Research Chair. He served as an Associate Editor of the IEEE TRANSACTIONS ON GEOSCIENCE AND REMOTE SENSING from 1996 to 2002.

Bo Huang (A'12) received the Ph.D. degree in remote sensing and mapping from the Institute of Remote Sensing Applications, Chinese Academy of Sciences, Beijing, China, in 1997.

He is currently a Professor with the Department of Geography and Resource Management, The Chinese University of Hong Kong, Shatin, Hong Kong, where he is also the Associate Director of the Institute of Space and Earth Information Science. Prior to this, he held faculty positions in the Schulich School of Engineering, University of Calgary, Calgary, AB, Canada (2004–2006), and the Department of Civil Engineering, National University of Singapore, Singapore (2001–2004). He serves as the Executive Editor of Annals of GIS and on the editorial boards of several international journals, including the International Journal of Geographical Information Science and the Journal of Remote Sensing. His research interests are broad, covering most aspects of geoinformation science, specifically spatiotemporal image fusion for environmental monitoring, spatial/spatiotemporal statistics for land-cover/land-use change modeling, and multiobjective spatial optimization for sustainable land-use planning. He is currently exploring along the line of precision remote sensing, convinced that this new paradigm will revolutionize the way how multisensor remotely sensed data are fused and exploited to improve the performance and quality of various applications in the future.

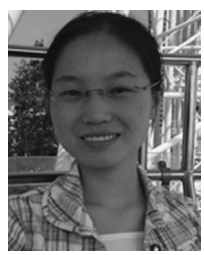

Huihui Song received the B.S. degree in technology and science of electronic information from the Ocean University of China, Qingdao, China, in 2008 and the M.S. degree in communication and information system from the University of Science and Technology of China, Hefei, China, in 2011. She is currently working toward the Ph.D. degree in the Department of Geography and Resource Management, The Chinese University of Hong Kong, Shatin, Hong Kong.

Her research interests include remote sensing image processing and image fusion.

Yiran Li received the B.S. degree in mathematics from Zhejiang University, Hangzhou, China, in 2010, and the M.Phil. degree in system engineering and engineering management from the Chinese University of Hong Kong, Hong Kong, in 2012.